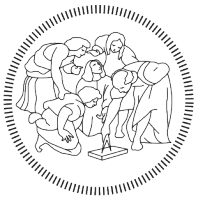

POLITECNICO
MILANO 1863

Bi-propellant liquid rocket motor for long term CubeSat missions

Name	Person Code	Matricola
Azzimonti, Nicolò	10724051	944328
Bassissi, Enrico	10538061	945090
Bologna, Andrea	10496997	943554
Colombo, Alessandro	10501045	946630
De Blasi, Francesca	10493834	946752
De Luca Maria, Alessandra	10520091	942711
di Trocchio, Marco	10545177	945944
Fiore, Walter	10531278	939473
Mucci, Marco	10535350	944931
Parisi, Adrian Burton	10710691	940789

Final Report of TEAMS ROCKET

Course of Space Propulsion
School of Industrial Engineering
Academic Year 2019-2020

Abstract

A compact hydrazine/hydrogen peroxide pressure-fed bi-propellant propulsion system for long term linear 4U CubeSat missions has been designed. The requirements of providing a Δv of 600m/s, containing a 1U payload of 1.33kg, and to not exceed an acceleration of $3g_0$ have been satisfied. The specific impulse was determined to be 332s with a given constant thrust of 10N. The design decisions for propellant choice has been justified via calculations using a NASA CEA software package, and operating principles and key design considerations for each component are outlined. A complete analysis of the thrust chamber was completed with material selected to maintain simplicity and increase reliability, and injector plate sizing performed. COTS components have been reviewed to aid in calculations and potential inclusion into the design. CAD drawings and schematics have been developed and failures modes considered and analysed leading to potential off design conditions.

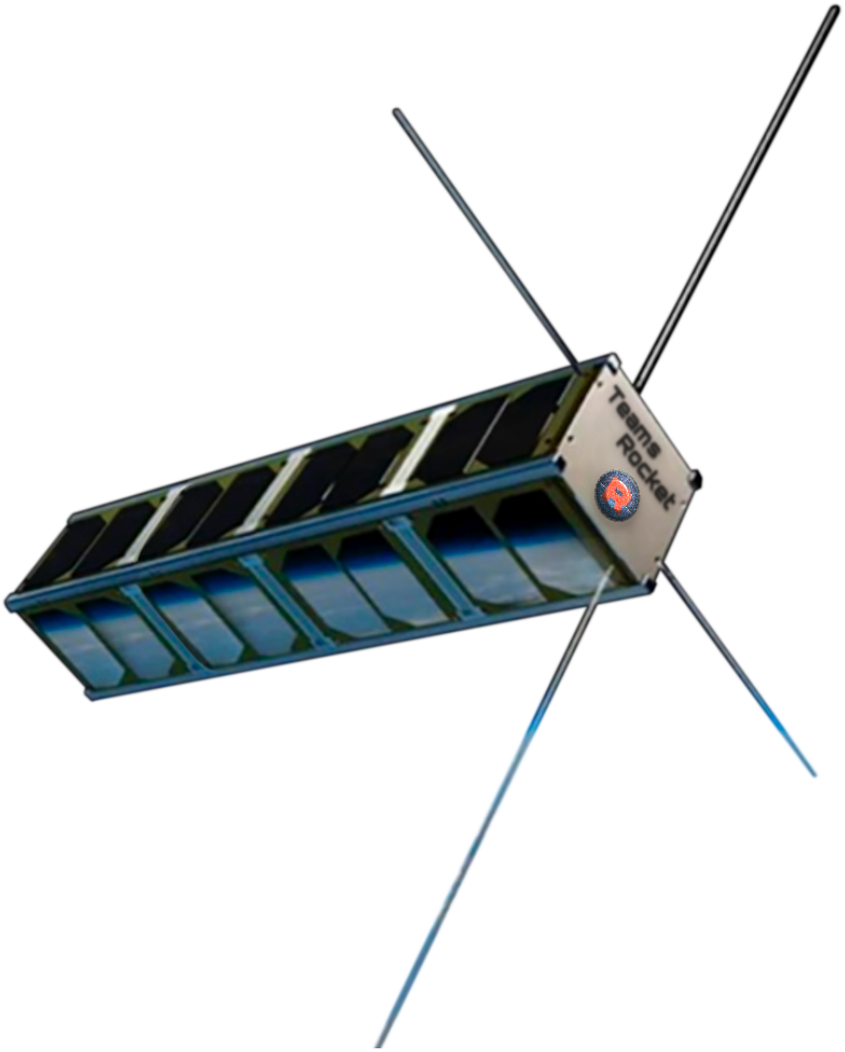

"To extend our reach to the stars above"

Contents

List of Figures

List of Tables

Nomenclature

β	Semi-apex angle	deg
$\dot{m}_p$	Propellant mass flow rate	kg/s
γ	Heat capacity ratio	-
λ	Thermal conductivity	W/m K
ν	Poission's ratio	-
ρ	Density	kg/m^3
θ_f	Final parabola angle	deg
θ_i	Initial parabola angle	deg
ε	Expansion ratio	-
A_c	Combustion Chamber Area	m^2
A_e	Exit area	m^2
A_t	Throat area	m^2
$A_{inj,i}$	Actual single injector area	m^2
A_{inj}	Chosen single injector area	m^2
A_i	Total areas of the orifices	m^2
c^*	Characteristic velocity	m/s
c_d	Discharge coefficient	-
c_F	Thrust coefficient	-
c_p	Specific heat	KJ / kg K
d_{inj}	Chosen injector diameter	m
E	Young modulus	GPa
F_{tu}	Ultimate tensile strength	GPa
g_0	Gravity acceleration at s. l.	m/s^2
I_s	Specific impulse	s
I_v	Volumetric sp. impulse	kg s / m^3
I_{tot}	Total impulse	N s
I_{vac}	Specific impulse in vacuum	m/s
L^*	Characteristic length	m
M_c	Combustion chamber Mach number	-
m_p	Propellant mass	kg
m_{dry}	Dry mass	kg
m_{fu}	Fuel mass	kg
M_{mol}	Molar mass	g / mol
m_{ox}	Oxidizer mass	kg
N_i	Injector's holes number	-
OF	Oxidizer to fuel ratio	-
P_b	Pressure burst	Pa
P_c	Combustion chamber pressure	bar
P_e	External pressure	Pa
P_{super}	Super - pressurised tank pressure	Pa
SF	Safety factor	-
T	Thrust	N
t	Thickness	mm
t_b	Burning time	s
T_c	Combustion chamber temperature	K
t_{ing}	Ignition delay time	s
t_{mix}	Mixing time	s
u_i	Injection velocity	m/s
V_c	Combustion Chamber Volume	m^3
v_e	Exit velocity	m/s
V_{fu}	Fuel volume	m^3
V_{ox}	Oxidizer volume	m^3

1. Introduction

CubeSats are a class of miniaturized satellites built in standard units of $10 \times 10 \times 10\text{cm}^3$ each, with no more than 1.33 kg of mass per unit [43]. This kind of nanosatellites facilitates frequent and affordable access to space with low cost; they are commonly put in orbit by deployers on the International Space Station [42], or launched as secondary payloads on a launch vehicle. The standard dimensions also allows CubeSats to hitch a ride to orbit within a container, which simplifies the accommodation on the launcher and minimises flight safety issues, increasing the number of launch opportunities as well as keeping the launch cost low. Moreover, due to their high degree of modularity and extensive use of commercial off the shelf subsystems, CubeSat projects can be readied for flight on a much more rapid basis compared to traditional satellite schedules, typically within one to two years [43].

Interplanetary CubeSat missions expand the horizon of CubeSat applications; in order to achieve that, robust primary propulsion systems become indispensable. The volume and mass constraints drive to simple propulsion systems. There are a plethora of available CubeSat propulsion systems designed for specific missions and orbits with systems varying from simple cold gas thrusters to more complex state of the art ion engines, and some utilising the sun as their source of thrust via solar sails [1].

This work focuses on the development of a liquid bipropellant chemical propulsion system for a single burn orbit transfer, analysing the state-of-the-art of such kind of CubeSat [3]. The following sections highlight the choice of the propellant and their corresponding properties, the design of tanks, feed system, thrust chamber, and nozzle and the corresponding performance values.

2. Design

The following chapter will cover the entire design process of the propulsion system with the proposed requirements in question.

2.1 Requirements and preliminary considerations

A bi-propellant propulsion system has been requested by PoliMi Space Agency to aid in the long-term mission of a 1U payload of weight 1.33kg. The main performance requirement is that the propulsion system has to provide a $\Delta v = 600 m/s$, with a maximum acceleration not exceeding $3g_0$. The propulsion system to be designed should consider the combustion chamber, nozzle, pipes, valves, and tanks spread amongst connected units within the CubeSat. It is assumed that the 1U payload contains the required power storage and capabilities of powering and controlling the propulsion system. No staging is expected to occur during operation and a single burn manoeuvre is assumed.

CubeSat main structures are typically made from an aluminium alloy. However, studies have been conducted by Ampatzoglou et al. on composite alternatives allowing for a lighter design [4]. Thus, a conservative empty structural mass of 133g per unit is considered.

Initial mass values of the components are required in order to aid with calculations. A literature review was conducted to estimate the rocket's dry mass, as shown in Table 2.1 [29] [5] [6] [38]. This estimated value will be used in an iterative design process in which the mass is adapted at each step to match mission requirements. The thrust, T, is assumed to be constant

and set to 10N, which can be found for other CubeSat applications [3] [37]; it satisfies the acceleration constraint as T_{max} is found to be

$$T_{max} = m_{dry} \cdot 3g_0 = 77.05N \tag{2.1}$$

Feed system mass	120 g	Payload mass	1330 g
Thrust chamber mass	350 g	Injection plate	100 g
Pressure regulator	76 g	Structural mass for 4 units	532 g
Electronic mass	200 g	Tank mass	120 g
		Total dry mass	**2.619 kg**

Table 2.1: Estimated mass of each component

2.2 Propellant Choice

Three propellant couples have been selected to undergo investigation: Nitrogen tetroxide (N_2O_4) and monomethylhydrazine (CH_6N_2), hydrogen peroxide (H_2O_2) and monomethylhydrazine, and hydrogen peroxide and hydrazine (N_2H_4). The properties of the aforementioned molecules are reported in Table 2.2.

	Oxidizers		**Fuels**	
	N_2O_4	H_2O_2	N_2H_4	CH_6N_2
Freezing point [K]	261.95	272.6	274.69	220.7
Boiling point [K]	294.3	423	386.66	360.9
Specific gravity [kg/m^3]	1.447	1.42	1.005	0.8788
Molar mass [kg/kmol]	92.016	32.4	32.05	46.072

Table 2.2: Comparison of characteristics between oxidiser and fuel candidates [31] [32] [33] [34]

The variation of the specific impulse in vacuum, I_{vac}, with respect to the oxidiser to fuel ratio, O/F, for each propellant is calculated via NASA CEA, a software packaged developed by Bonnie J. McBride at NASA Glenn Research Center [35]. The expansion ratio and combustion chamber pressure were fixed at 100 and 10 bar, respectively, with the assumption of infinite area and frozen condition imposed at the combustor. The results can be seen in Figure 2.1(a).

The candidates propellants are storable which satisfy the requirements regarding the long term aspect of the mission and are hypergolic, reducing the complexity of the engine as ignition systems are not necessary [34]. Hydrazine and hydrogen peroxide couple was chosen for the propulsion system. This took into account the high I_{vac} and relatively high densities leading to more compact tanks. In addition, this couple allows an high temperature range for the pressurising gas expansion. Furthermore, the oxidizer is 90% w/w H_2O_2 in water to avoid

toxicity, incompatibility and corrosion problems while still guaranteeing high performances [29].

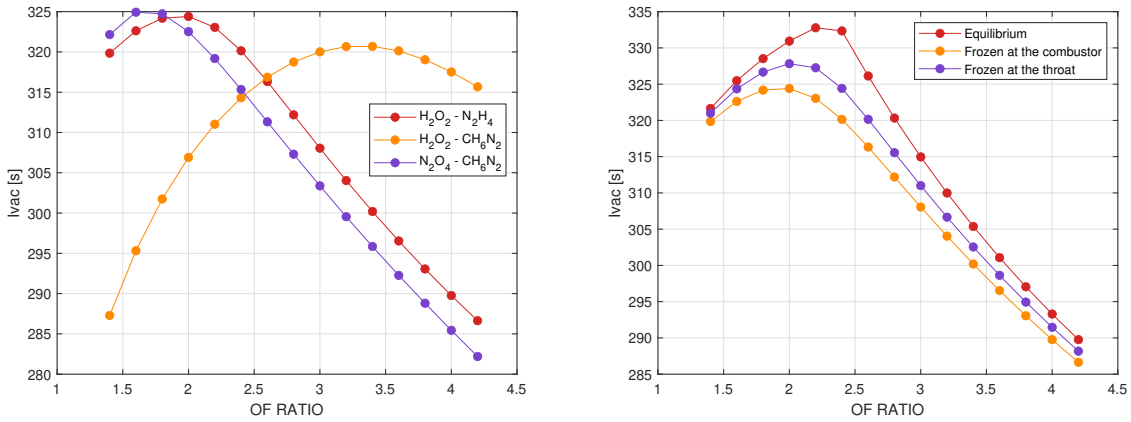

(a) Specific impulse variation with OF for the three propellant candidates.

(b) Specific impulse variation with OF in the three conditions.

Figure 2.1: Calculations performed within NASA CEA software package

2.3 Thermodynamic analysis and characteristic parameters

Once the propellant has been selected, some design parameters have been set according to the structure and the propulsion system under development. The expansion ratio, ε, and combustion chamber pressure, P_c, have been fixed following a literature review of similar sized propulsion systems design by Topputo et al. and in the Rosetta mission [3] [37].

$$P_c = 10\,\text{bar} \qquad \varepsilon = 100$$

Performances corresponding to these fixed values with the chosen propellant were calculated within the aforementioned CEA code and carried out within three different conditions: equilibrium, frozen at the combustor and frozen at the throat.

As shown in Figure 2.1(b), the equilibrium condition provides an overestimation of the performance parameters, since both dissociation and recombination reactions are considered. In contrast, the frozen condition in the combustor provides an underestimated result due to the lack of recombination reactions in the nozzle. Hence, the frozen condition at the throat was selected as it represents an intermediate solution. Non-isentropic phenomena have not been considered within these calculations. The chosen OF ratio corresponds to the maximum of the specific impulse for the selected curve; however, this value of I_s is reduced to an efficiency of 99% to take into account any possible losses. All the other parameters obtained through CEA are reported in Table 2.3.

OF	I_s [s]	C_p [kJ/kgK]	M_{mol} [kg/kmol]	Tc [K]	c^* [m/s]	γ [−] [1]
2	332.33	3.4750	18.934	2653.05	1689.1	1.1446

Table 2.3: Calculated thermodynamics parameters.

An iterative approach was performed to determine the ratio P_e/P_c with an error tolerance of 1‰. Once converged, the exit pressure and velocity, and parameters of merit can be calculated using common thermodynamic relations [3]. The results of which can be seen in Table 2.4.

P_e [Pa]	v_e [m/s]	c_F [−]
854.5	3299.7	1.949

Table 2.4: Performance parameters.

A_t [mm^2]	A_e [mm^2]	$\dot{m}_p$ [kg/s]	t_b [s]
5.1307	513.07	0.003	180.54

Table 2.5: Physical parameters.

Using the Δv requirement mentioned in Sect. 2.1, v_e, the dry mass of the satellite and a safety factor SF of 5%, the propellant mass m_p can be determined through the Tsiolkovsky equation:

$$m_p = m_{dry} \cdot (\exp(\Delta v/v_e) - 1) \cdot SF = 548.4\,\text{g} \tag{2.2}$$

Exploiting the values of Table 2.3 and 2.4, the throat and exit areas, A_t and A_e, respectively, the propellant mass flow rate, $\dot{m}_p$, and the burning time, t_b, have been computed and shown in Table 2.5.

2.4 Tank Analysis

Each tank must be sized in order to have the volume corresponding to the adequate propellant mass for the propulsion to surpass the requirements. The individual oxidiser and fuel masses were then determined with use of the oxidiser to fuel ratio decided within Sect. 2.2, denoted as OF in the following equations.

$$m_{ox} = m_p \cdot (OF/(1 + OF)) = 365.6\,\text{g} \tag{2.3}$$

$$m_{fu} = m_p \cdot (1/(1 + OF)) = 182.8\,\text{g} \tag{2.4}$$

With use of the densities presented in Table 2.2 the relative volume to each propellant can be derived. An additional safety factor of 3% was introduced to account for temperature variations whilst within an operational environment.

$$V_{ox} = m_{ox} \cdot \rho_{H_2O_2} \cdot 1.03 = 0.26897\,\text{dm}^3 \tag{2.5}$$

$$V_{fu} = m_{fu} \cdot \rho_{N_2H_4} \cdot 1.03 = 0.18734\,\text{dm}^3 \tag{2.6}$$

Risk of vaporisation of the propellants is not of concern since the boiling points are above the operational temperature of typical on-board electronics temperature limits. [18].

Additional insulation is proposed in order to keep the temperature of the propellants within a suitable range. Mylar® insulating film has been chosen, for its low thermal conductivity of $\lambda = 0.14\text{W/mK}$, and wide operating temperature range of $200\text{K} - 425\text{K}$, and the density $\rho = 1.39\text{g/cm}^3$ that, with an adequate covering, leads to a negligible additional weight [2].

PRTs[2], also with a negligible mass, can be used to monitor temperature of the tanks. Simple heaters composed of electrical resistance elements can be used as an active thermal control, but a further development will be left for future projects.

The fuel and oxidiser tank pressures were found by analysing the pressure cascade from the combustion chamber to each corresponding tank. The velocities within the feed lines were assumed to be $u = 10\text{m/s}$. The resulting pressure drops are reported in Table 2.6.

[1]The heat capacity ratio is computed with the following formula $\gamma = C_p/(C_p - R/M_{mol})$ where R is the universal gas constant.

[2]Standard Platinum Resistance Thermometers (Standard SPRTs)

Component	Injectors	Feed Lines	Dynamic Losses Ox	Dynamic Losses Fu
ΔP [bar]	$0.2P_c = 2$	$0.05P_c = 0.5$	$\frac{1}{2}\rho_{ox}u^2 = 0.7$	$\frac{1}{2}\rho_{fu}u^2 = 0.5025$

Table 2.6: Pressure Losses in the Feeding System

Two different tank configurations were considered in parallel, spherical tanks and cylindrical-like tanks. The geometry of the cylindrical-like tank consists of a body radius of 4.5cm with two caps at both ends. The height of the caps is scaled accordingly to the length of the cylinder.

To better explain the cylindrical-like shape, the dimensions and volumes of the maximum tank that can stay in 1U structure with this guidelines, are taken as reference. The total height would be 9.352cm with an optimized volume available inside of 0.484dm^3, instead of a sphere of radius 4.5cm and corresponding volume of 0.3817dm^3.

The tank structural material was chosen to be Ti-6Al-4V. The main two considerations for the choice were the corrosion resistance against the chosen propellants, and the high strength to weight ratio of the material. In addition, the collective manufacturing knowledge regarding this alloy, multitude of available manufacturing processes, and the availability of the material further justifies this decision.

ρ [kg/m^3]	F_{tu} [GPa]	E [GPa]	ν[−]
4460	1.23	113.8	0.342

Table 2.7: Mechanical properties of Ti-6Al-4V [7] [17] [15] [14]

The thickness of the tanks were determined using Barlow's formula with the burst pressure obtained by considering a safety factor SF = 4 with respect to the operating storage pressure. The radius of the spherical tank was used and the ultimate tensile strength of the chosen material. The calculated dimensions for each configuration are shown Table 2.8.

	Spherical		**Cylindrical**	
	Fuel	**Oxidizer**	**Fuel**	**Oxidizer**
Radius [dm]	0.3550	0.4004	0.45	0.45
Height [dm]	-	-	0.5213	0.3633
Exit Surface [dm^2]	1.5834	2.0221	0.9180	1.2987
Thickness [mm]	0.0751	0.0860	-	-
Tank Mass [g]	5.2997	7.7244	3.0057	4.9399

Table 2.8: Spherical and Cylindrical Fuel/Oxidizer Tanks Comparison

As reported in Table 2.8 there are no values for the thicknesses of cylindrical tanks because this first approximation analysis is conducted applying Barlow's spherical burst formula to both cases in order to have a valid estimate value of the thickness. Further analysis would be required to have a more precise value to specify more clear-cut masses and volumes.

From Table 2.8 the masses of the tanks are shown to be relatively small with respect to the propellant they contain therefore, all considerations are focused to minimise the occupied volume

of the propellant. It is clear that if spherical tanks are to be utilised the positioning of fuel and oxidiser tank within the same unit would exceed the maximum dimensions. The cylindrical-like tanks would enable the possibility of containing both the oxidiser and fuel tank within the same unit with a combined height of 8.84cm (being $h_{cyl_{fu}} = 3.63$cm and $h_{cyl_{ox}} = 5.21$cm) and radius fixed as usual at 4.50cm.

2.5 Pressurising Gas

Typically there are two candidates in regards to a pressurising gas, N_2 and He, due to their inert nature. N_2 was decided on account for higher density, in the aim for a more compact design, in addition to the low cost in comparison to He.

The low thrust requirement led to the decision of incorporating a pressure-fed design. A pressure fed device can ensure high pressure tanks with a small amount of pressurising gas whilst maintaining simplicity. Moreover, as the thrust must be maintained constant in operative conditions therefore, a blow-down system can not be used.

Several different configurations were considered however, a system with a single pressurising tank supplying both oxidiser and fuel tanks was opted for. A system containing two pressurisation tanks, although providing an option for additional redundancy, leads to high volume occupancy and diverges from the desired compact design.

The initial temperature prior to burn was set to an upper operating limit of 327K, taking into account of thermal limits of electronic components and the temperatures reached within a space environment [21]. The final temperature is set to 2K above the freezing point of N_2H_4. In order to supply sufficient pressure for both propellant tanks at end of activity, the initial gas pressure in the tank was found to be 23.59 bar. This value would lead to a corresponding volume of 0.8874dm^3 which would exceed the available tank volume of one unit. Given the fact that the pressure is quite small, a super-compression strategy has been carried forward: in order to fit exactly the volume of the maximum cylindrical-like tank that can fit into 1U, i.e. 0.4835dm^3, a super-pressurization up to $P_{super} = 43.30$ bar is obtained. Just for comparison, it is here reported also the super-pressure of the equivalent maximum spherical tank that can fit 1U, 54.8565 bar, so the first configuration has been chosen because it obtains the lowest losses into the isenthalpic pressure regulator due to the lower pressure.

The tank volume was calculated similarly to the propellant tanks with dimensions of a cylindrical-like shape with radius and total length of 4.50 cm and 9.36 cm, respectively. This allows for a more efficient use of volume. The thickness of tank, utilising the same alloy as the propellant tanks and a safety factor of 4, was found to be

$$t = \frac{P_b \cdot r_t}{2F_{tu\ Ti}} = 0.343\text{mm} \tag{2.7}$$

where P_b is the $P_{super} \cdot$ SF. Together this results in a inert gas mass of 22.6 g and a tank mass of 49.4 g.

2.6 Thrust Chamber and Nozzle

The thrust chamber presents a bell-shaped nozzle modelled through the Rao approximation [23]. The curves have been interpolated to obtain the angles for an $\varepsilon = 100$, as chosen in fig. 2.3. The divergent is 34.34 mm, which is 80% of the Rao conical length, with a 2D loss of 0.1% leading

to a value of thrust equal to 9.989 N. It was established that the viscous effect does not impact the performance of the nozzle, as seen in Appendix A.1.

Imposing a low $M_c = 0.03$ the contraction ratio was computed to be $A_c/A_t = 19.87$, where A_c and M_c are the area of combustion chamber and mach within the combustion chamber, respectively. This supports the assumption of infinite combustion chamber area used in the aforementioned CEA software package [29]. Fixing the semi-apex angle $\beta = 40°$, it drives the length of the convergent part to be equal to 5.27 mm.

The sizing of the combustion chamber is carried out with the aim of assuring complete mixing and combustion. The range of the optimal characteristic length L^* for hydrogen peroxide/hydrazine is assumed to be the same for nitrogen tetroxide/hydrazine-base fuel, due to similar hypergolic behaviours [24].

In particular, it is considered L^* equal to 30in (0.76 m). The combustion chamber is shaped as a cylinder whose dimensions are computed from the following equations:

$$V_c = L^* A_t \qquad L_c = \frac{V_c}{A_c} \tag{2.8}$$

where $V_c = 7.3\text{cm}^3$, $A_c = 1.02\text{cm}^2$, $L_c = 37.74\text{mm}$. The thrust chamber is modelled on the basis of the Rao approximations which can be found in Appendix A.2.

Conv. length [mm]	5.27
Div. length [mm]	34.34
D_t [mm]	2.56
D_e [mm]	25.56
θ_f	7°
θ_i	33.8°
β	40°

L* [mm]	760
C.C. length [mm]	37.74
C.C diameter [mm]	11.39

Tot. length [mm]	77.34
Empty vol. [dm^3]	0.1943
Tot. mass [kg]	0.7185
Thickness [mm]	3.94
λ	0.999

Table 2.9: Thrust Chamber Parameters with C.C. representing the Combustion Chamber.

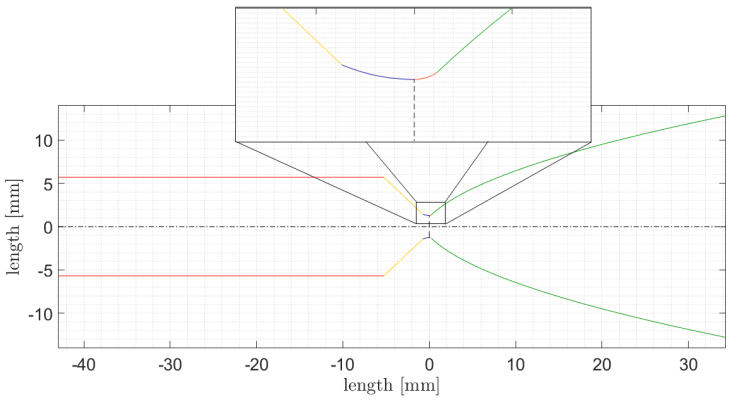

Figure 2.2: Modelled thruster profile based on Rao's curves using MATLAB®(Appendix A.2)

The thrust chamber faces high temperatures and strong stresses. To withstand these extreme conditions, it is proposed the structural material is to be Ir-10 wt % Re [3], whose density is 22.40 g/cm^3. This alloy presents a melting point above 2700 K and has been widely tested for NTO/MMH, successfully resisting to corrosion; further details can be found in Appendix A.3.

[3]No certainty on oxidation resistance for Rhenium diffusion above 20%.

The density of Hafnium dioxide, HfO_2 is 9.68 g/cm^3 and can be utilised as additional coating on account of its large thermal resistance [26].

Experiments have shown that a 0.84 mm thick HfO_2 coating provides a temperature drop of 574 K as shown in Figure 2.4(a) [27]. To reduce the external wall temperature to 300 K, in order to not overheat the surrounding structure and electronics, a 3.44 mm oxide coating is implemented with a 0.5 mm thick Iridium-Rhenium layer similar to that seen in Figure 2.4(b). This thickness respects the minimum one computed with Barlow's formula, which is 0.04 mm, considering the ultimate tensile strength of Iridium [28]. Due to the differences in the density of the layers, the mass is estimated with respect to the heavier density.

Therefore, a cooling system is not required providing a more compact, simple, and reliable system. This choice is supported by pre-existing cases [29].

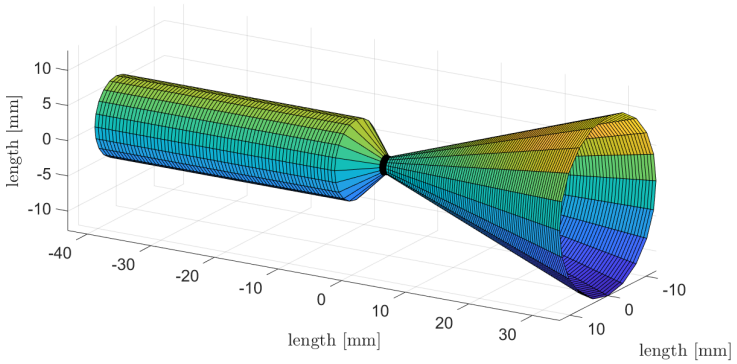

Figure 2.3: 3D view of the thrust chamber using MATLAB®

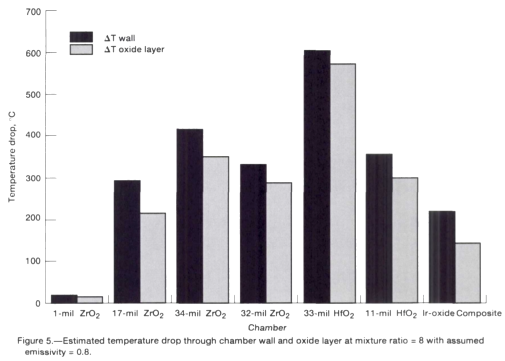

(a) Temperature drop with Hafnium Dioxide

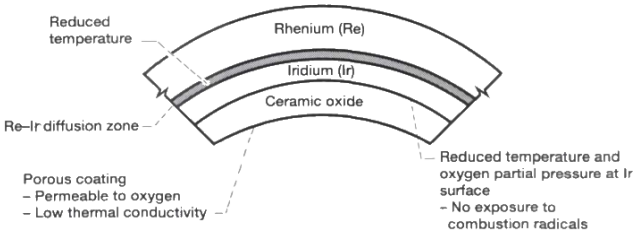

(b) Thrust chamber layers

Figure 2.4: Oxide-coated Iridium/Rhenium thrust chamber

2.7 Injector Sizing

Hypergolic ignition is a critical point in the development of the system, because the impingement of hypergolic streams is often concerned with the observed explosions near the injection plate since they can act as initiation sources of denotation waves or "pops". The total hypergolic ignition can be broken down into an ignition delay time t_{ign} and a mixing time t_{mix}. The criteria for the jet separation can be stated as $t_{ign} \leq t_{mix}$. The t_{mix} is a function of the stream diameter, the velocity, and the impingement angle. It is reasonable to assume a mixing stream model and

to not concern about "popping" and stream separation due to low diameter and velocity values [19].

It is observed that injector poppings occur more frequently using larger orifice diameters at lower chamber pressures and less frequently using smaller orifice diameters at higher chamber pressures. Moreover, the choice of a liquid/liquid injection is justified by the fact that an injection in a gaseous and a liquid phase leads more frequently to a separated flow, because the vapor stream carries the liquid droplets along with it, confining the liquid droplets mainly on the fuel side [16].

Since this system uses a hypergolic couple, unlike injectors can easily cause failure. Therefore a like-on-like injector is used, even though the mixing happens further along the stream. This penalty on the delay of the mixing is balanced by the fact that hypergolic propellants react faster with respect to normal propellants. In particular, the chosen configuration of injection is 2 OX : 1 FU, since the OF is equal to 2.

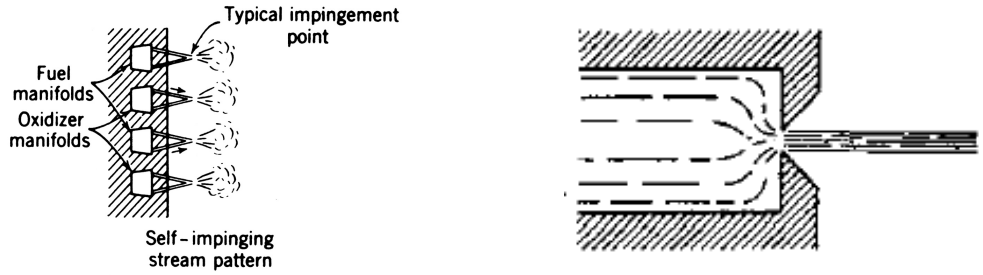

(a) Like-on-like injector

(b) Sharp-edged orifice

Figure 2.5: Injection design [29]

The pressure drop, ΔP, of the injection is assumed to be in the typical range for a like-on-like injector (15% - 25%) thus, $\Delta P = 0.2Pc = 200\,\text{kPa}$.

A sharp-edged orifice is chosen since due to ease of manufacturing, consistent with the aim of this technology, with a diameter of $d_{inj} = 0.1\text{mm}$ ($A_{inj} = 7.8540 \cdot 10^{-3}\text{mm}^2$) and a Cd = 0.6 because roughness leads to a small decrease of the discharge coefficient. [29][36] The maximum feasible angle from a manufacturing viewpoint is 45° [41], the injection angles are selected equal to 40° both for the oxidizer and the fuel, in order to increase the mixing efficiency.

The total area of the orifices necessary to discharge the correct mass flow rates is given by (i denotes either the oxidiser or fuel):

$$A_i = \frac{\dot{m}_i}{C_d\sqrt{(2 \cdot \Delta P \cdot \rho_i)}} \tag{2.9}$$

Computing the number of holes for either the oxidizer and fuel injectors, were found to be $N_{fu} = A_f/A_{inj} = 11$ and $N_{ox} = A_{ox}/A_{inj} = 19$.

In order to match the problem constraint 2 OX:1 FU, we select $N_{ox} = 20$ and $N_{fu} = 10$. The individual injector areas can be ascertained via $A_{inj_i} = A_i \,/\, N_i$ and the results for each propellant can be seen in Table 2.10.

It can be observed that the values are quite similar therefore, it is reasonable to assume the same discharge coefficient. The injection velocities are computed via

$$u_i = Cd \cdot \sqrt{\frac{2 \cdot \Delta P}{\rho_i}} \tag{2.10}$$

	Count	$A_i[mm^2]$	$A_{inj,i}[mm^2]$	$d_{inj,i}[mm]$	$u_i[m/s]$
Oxidizer	20	$1.4262 \cdot 10^{-1}$	$7.1311 \cdot 10^{-3}$	$9.5287 \cdot 10^{-2}$	10.1419
Fuel	10	$8.4166 \cdot 10^{-2}$	$8.4166 \cdot 10^{-3}$	$1.0352 \cdot 10^{-1}$	11.9701

Table 2.10: Oxidizer and fuel injection properties

2.8 Feed System

To provide the desired feeding from the pressurized N_2 tank, a manually adjustable COTS[4] three-staged pressure regulator was used. The regulator taken into account was designed to handle variable inlet pressure up to 200 bar, while consistently regulating to pressures to a fine accuracy. The overall mass of the regulator is 76g while the diameter is $\approx$ 26mm and the height is $\approx$ 34mm [5].

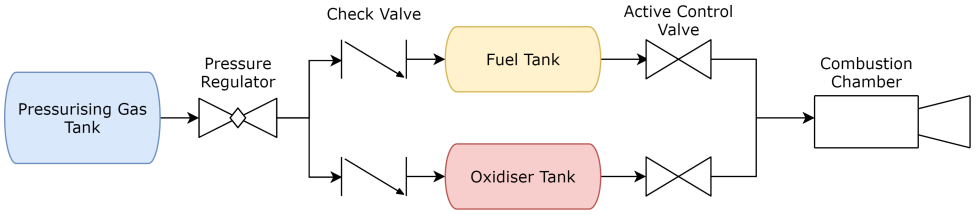

Figure 2.6: Schematic of the propellant feed system

Given that the design is acceptable in terms of dimensions, it has to be adjusted to work with our pressure values. The gas in the regulator performs isenthalpic expansions, and is subjected to a temperature drop due to Joule-Thompson effect, however reduced by the multiple stages. The use of pressure transducers and valves is essential for the proper operation of the feed system, and an approximation of their masses was considered in the calculations [10]. Check valves control the fluid flow through the system, guaranteeing flow in only one direction. COTS microfluidic active control valves can be utilised to control amount of flow moving through the system and remains closed until powered. Control actions will be based on the readings received from the pressure transducers set before and after the pressure regulator. Additional fill/vent valves are required within the system however, have not been included due to the current design phase.

Finally an all-weld piping train will be used to reduce the number of compression fittings, potential leak sources, and reduce the mass of the the propellant management system, reaching an overall mass for the whole train of around 100g [6].

2.9 Configuration and Performances summary

Three units will be dedicated to the propulsion system while one unit will house the payload resulting in a 4U linear CubeSat. Each component must be restrained in only one unit hence an optimized configuration should exploit the available space. One unit is to be dedicated to the thrust chamber consisting of the injection plate, combustion chamber, and nozzle.

The remaining available space can be used to store the pressure regulator and thus, the adjacent unit will contain the pressurising gas tank. The remaining unit will contain the fuel and oxidizer tanks. Once the configuration was set, the dry mass has been computed again

[4]COTS:Commercial Off-the-Shelf component

considering the actual masses of all the subsystems in accordance to an iterative design process. The final value obtained for the CubeSat dry mass is $m_{dry} = 2.62$kg, which confirms the Δv requested for the mission. An approximated evaluation of the Centre of Gravity (CoG) has been

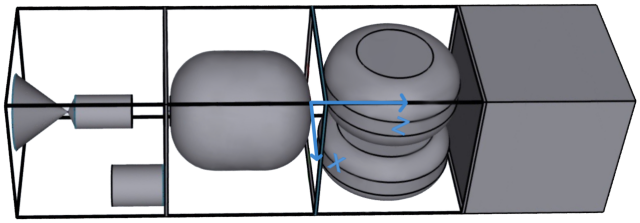

Figure 2.7: Schematic configuration of the CubeSat obtained with Siemens Shapr3D® CAD

done for both the case of full tanks and after the firing. The CoG of each component has been considered to lay in the geometric centre of the component itself, exception made for the nozzle which has been simply considered as a cone. The CoG, according to the reference frame in figure, has a distance $z_{empty} = -3.3$cm and $z_{full} = -1.7$cm from the centre of the satellite along the Z axis, and a distance $x_{empty} = -0.045$mm and $x_{full} = -0.037$mm from the centre along the X axis. It is assumed to be in the centre of the satellite for what concern the Y axis since the only asymmetric component is the pressure regulator, which has a negligible mass with respect to the whole satellite. Being the CoG close to the geometric centre of the satellite itself a minor control effort should be used to manage the attitude while firing with the main propulsion unit. Moreover, it can be noticed that the values obtained satisfy the criteria expressed in [30], which require a location of the CoG within 4.5cm in the X direction and 7cm in the Z direction from the geometric centre.

Concerning the performance parameters, keeping into account the 2D losses, the main values obtained are listed in Table 2.11.

T [N]	I_s[s]	I_v [g · s/cm^3]	I_{tot} [N · s]	Δv [m/s]
9.989	332.33	411.37	1803.5	600

Table 2.11: Summary of performance parameters

2.10 Failure Modes

CubeSats tend to consist of a plethora of microprocessors and electronic circuitry. These components are utilised for control and monitoring of the spacecraft and for functionality of the payload. As most small satellites do not contain radiation hardened components, failures are not uncommon.

The definition of the failure of a small satellite is not as clear in comparison to that of a launcher failure. As described by Jackin, these failures can be condensed into two categories *mission failure*, and *partial mission failure*. The majority of all failures within small satellites tend to be of an electronic nature and total mission failures tend to occur before the mission begins with numerous satellites showing no form of communication post-deployment [13]. The failure modes solely affecting the propulsion system will be discussed.

The propulsion system electronic control board, when comparing to the most recent history regarding small satellite failures, is most likely to fail. Bouwmeester describes common communication failures on I2C bus interfaces between boards, thus incorrect firings or lack of,

can cause issues when attempting a manoeuvre [12]. Furthermore, exposure to the radiation of space and the lack of radiation hardened components can lead to bit shifting within electronic components and thus, unexpected behaviour of the propulsion system [22].

The satellite is assumed to be subjected to temperature ranges due to non-constant exposure to the sun during orbit. These temperatures can range from -120°C to 120°C. The satellite may not reach these lower temperatures due to thermal inertia of the system, the orbital period of the satellite, and other components within the satellite generating heat. The thermal cycles experienced by the tank over a long mission, coupled with the high pressures required for the pressurising gas, could in turn cause a structural failure leading to the loss of the satellite and thus, total failure of the mission [11] [21].

Valves typically have two different outcomes to a failure: *fail-open* and *fail-closed*. The utilisation of *fail-open* valves, upon failure, could conduct an unsolicited uncontrolled burn and increase the likelihood of a failure of the mission. Therefore, *fail-closed* valves would add a safe-guard taking this into consideration, although limiting to only one propellant, with the spacecraft remaining under control of the operator. Under the failure of one of the control valves or check valves can lead to an off-design condition effectively altering the propulsion system into a cold gas thruster with reduced Δv capabilities reducing the likelihood of a total mission failure [8] [9].

3. Conclusion

To conclude, a 3U propulsion system has been developed for a 4U linear CubeSat with payload of size 1U and weight 1.33kg with all requirements satisfied. The final propellant choice, hydrazine/hydrogen peroxide, was decided from three candidates and chosen due to the calculated performance values and collectively higher density. Thermodynamic analyses were conducted via a NASA CEA software package to determine performance calculations along with common thermodynamic relations.

Tank dimensions and masses were calculated and justified given the proposed configuration, a pressure-fed system with one pressurised tank containing N_2 to supply an operating pressure for both propellant tanks. The final tank material choice was made to be Ti-6Al-4V on account to a high strength-to-weight ratio and corrosion resistance against the final propellant choice. The required pressurising gas pressure was additionally determined taking into account of phase change of the propellants and was found to be 43.3 bar.

The complete thrust unit has been sized and determined. A complete material analysis has been conducted and final material choices made to comply with temperature and pressure limits within the spacecraft. In particular, the internal layer of the thrust chamber is made of Hafnium dioxide to slow the corrosion and impose a temperature drop and an Iridium-Rhenium alloy composes the external layer of the thrust chamber to provide structural and thermal resistance. The injector plate analysis has also been performed resulting in a count of 20 and 10 injectors for the oxidiser and fuel, respectively, with diameters of $9.53 \cdot 10^{-2}$mm and $1.03 \cdot 10^{-1}$mm for the oxidiser and fuel, respectively.

The inclusion of valves within the feed system were also investigated with COTS components proposed and CoG calculations performed to ensure a base knowledge of resulting performance due to placement of components and were determined to not cause any concerning issues.

Further analysis must be made in order to verify and improve the design of the proposed propulsion system. Additional simulations and experiments can be made in the future to solidify the design choices made and operational components such as maintenance valves to be incorporated in forthcoming revisions.

Appendix

A.1 Viscosity displacement thickness

The team has examined the manner in with viscous effects influence the nozzle mass flow rate. Viscous effects retard the flow near the wall creating a boundary layer with a corresponding displacement thickness, δ^*. The displacement thickness decreases the actual area through which the mass can flow thus creating a decrease in mass flow rate. An assortment of boundary layer methods has been developed to estimate the throat displacement thickness for nozzle flows. The method considered here, is one developed separately by both Tang and Fenn[39] and Geropp[1] [40] that supplies the following expression for the viscous discharge coefficient:

$$C_D = 1 - \left(\frac{\gamma+1}{2}\right)^{\frac{3}{4}} \left[3.266 - \frac{2.128}{\gamma+1}\right] R_e^{'\,-\frac{1}{2}} + 0.9428 \frac{(\gamma-1)(\gamma+2)}{(\gamma+1)^{\frac{1}{2}}} R_e^{'\,-1}$$
$$R_e^{'} = R_{edyn}\sqrt{\frac{R_t}{R_l}} \tag{1}$$

where R_l is the radius of curvature at throat taken from Appendix A.2 as $1.5R_t$ and $R_e^{'}$ is a modified Reynolds number.

The viscous effect as to be analysed since the team is dealing with small components and in particular small throat area. If at throat the displacement thickness is comparable to throat radius it has a catastrofic effect. The computation of displacement thickness is related to the discharge coefficient through the following equation:

$$C_D = \frac{\dot{m}_{real}}{\dot{m}_{ideal}} \approx \frac{A_{effective}}{A_{throat}} \approx \left(\frac{R_t - \delta^*}{R_t}\right)^2 \tag{2}$$

In the analysed case the viscous effect does not impact the performance of the nozzle and in particular the results obtained is shown in table A.1.1:

Viscosity, μ [Pa s]	$R_e^{'}$	C_D	δ^* [mm]	$\frac{\delta^*}{R_t}$
8.9x10^{-5}	1.656x10^7	0.99941	0.0015	0.0012

Table A.1.1: Viscosity Analysis

[1]The expression of Tang and Fenn, for the viscous discharge coefficient, is identical to Geropp's with the exception that it includes an additional term that is inversely proportional to the Reynolds number.

A.2 Bell Shaped Nozzle contour

The divergent part of the nozzle is designed through the Rao's curves. A Thrust Optimized Parabolic Contours is constructed using three curves based on **Rao's approximation** [20]: an initial large circle from the combustion chamber to the throat, a smaller circle exiting the throat and a parabola to extend the approximated bell contour to the exit plane.

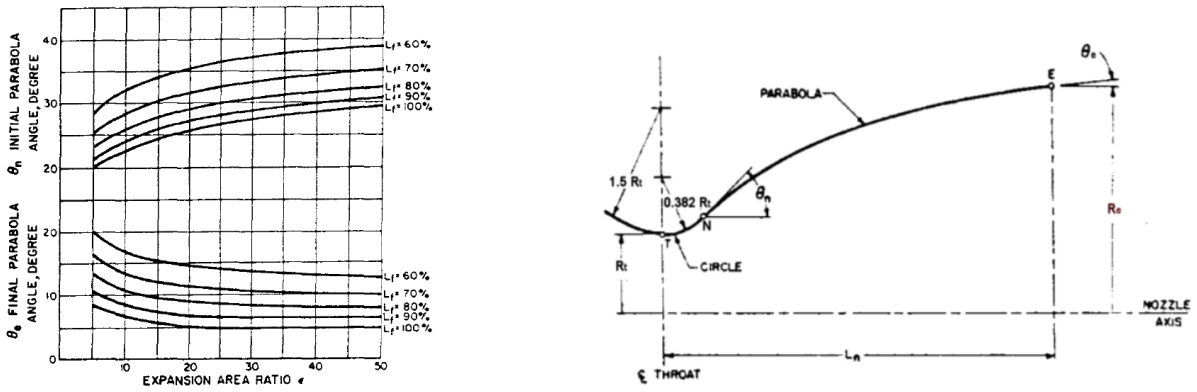

(a) Rao curves [29]

(b) Bell profile [20]

Figure A.2.1: Thrust Optimised Parabolic Contours based on Rao's approximation

The Rao nozzle starts with Rao's preferred throat geometry where he worked the optimisation process Fig. Using Rao coefficients to define the circular curves entering and exiting the throat, equal to 1.5Rt and 0.382Rt, was used as a baseline nozzle for this design.

The curves in Fig.A.2.1 (b) were modeled using MATLAB® starting from the data set.

The first two curves are designed to obtain a zero derivative without discontinuity in the throat. The first curve is determined as:

$$x^2 + (y - (R_t + 1.5R_t))^2 = (1.5R_t)^2 \tag{3}$$

which can then be solved for y:

$$y = -\sqrt{((1.5R_t)^2 - x^2)} + 2.5R_t \tag{4}$$

The second curve is also a circle computed in function of a smaller curvature of $0.328R_t$ and θ_{in}:

$$\begin{aligned} x &= 0.382R_t \cos\theta \\ y &= 0.382R_t \sin\theta + 0.382R_t + R_t \\ where &: -90^\circ \leq \theta \leq \theta_{in} - 90^\circ \end{aligned} \tag{5}$$

the final point (x_N,y_N) of the second circle has the same inclination of the initial point of the third curve defined as a parabola:

$$x = ay^2 + by + c \tag{6}$$

and the coefficients are computed through Boundary conditions that can be defined in a linear system such that:

$$\begin{bmatrix} y_N^2 & y_N & 1 \\ R_e^2 & R_e & 1 \\ 2R_N & 1 & 0 \end{bmatrix} \begin{Bmatrix} a \\ b \\ c \end{Bmatrix} = \begin{Bmatrix} x_N \\ L_{div} \\ \frac{1}{\tan\theta_{in}} \end{Bmatrix} \tag{7}$$

Reversing this linear system it is possible to obtain the value for the bell shaped nozzle. Part of the nozzle is shown in fig. A.2.3 to underline the difference between the three curves.

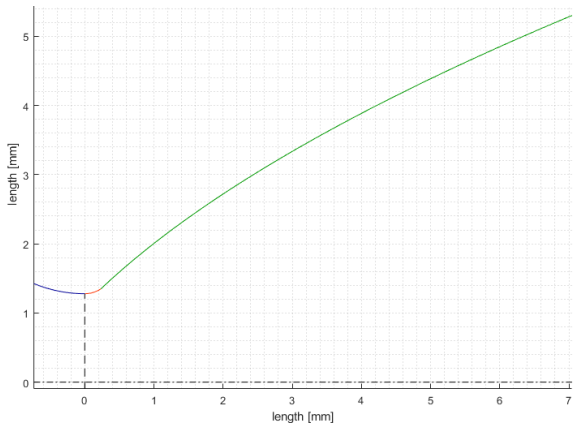

Figure A.2.2: 2D view based on Rao's approximation using MATLAB®

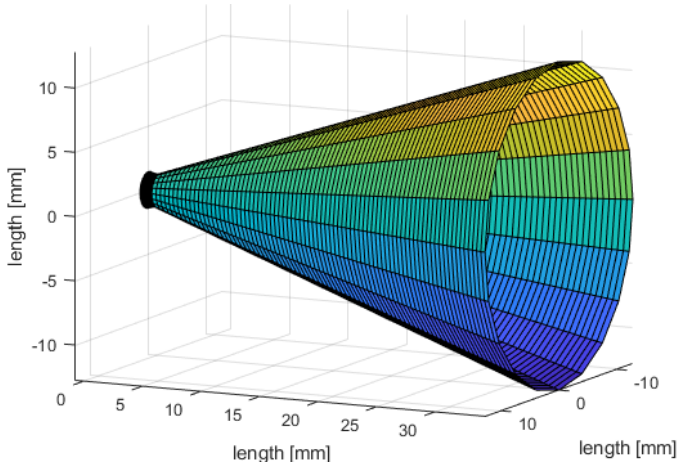

Figure A.2.3: 3D view based on Rao's approximation using MATLAB®

A.3 Iridium-Rhenium alloys data

Several tests have been made on Iridium-Rhenium alloys. This interest arises from the comparison with the main alternative for thrust chamber composition: niobium alloy. In fact, niobium alloys are lighter than Ir/Re alloys and widely used in small thrusters [3], but they require a cooling system, like a fuel film cooling system. Ir/Re can withstand higher temperatures than Niobium. This fact is exposed in a NASA document [25]. Then, it is considered the resistance of Ir/Re to oxidation at high temperatures. In Fig A.3.1 it is shown the data of a firing test whose goal was to study the corrosion rate on a Ir/Re thrust chamber. The test lasted for 15 hours at a constant outer-wall temperature of 2200 °C with a MMH/NTO propellant couple for a steady thrust of 22 N. No sensible damage was observed. Moreover, fig.**??** highlights a corrosion rate of few μm per hour (a range from 16.4 to 412 depending on the alloy composition) leading to no sensible damage to the thrust chamber within the time interval set by our burning time.

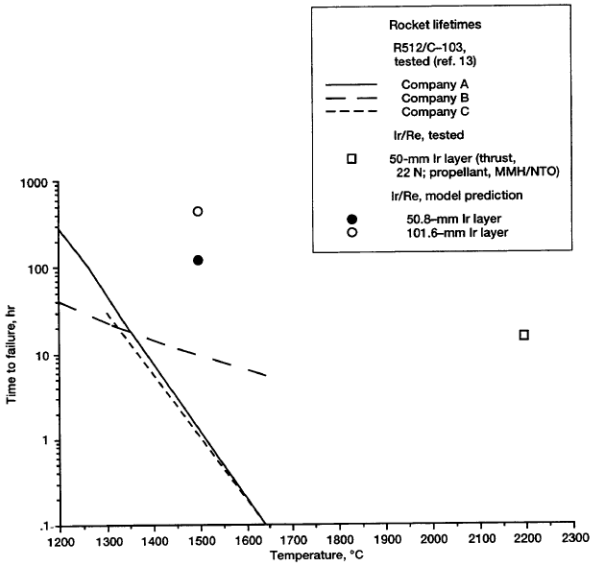

(a) Failure time

Alloy composition, wt %	Temperature, °C	Oxygen partial pressure, kPa	Recession rate, μm/hr
Ir-10Re	2200	7.7 (0.36 atm air-argon)	16.4
	2295		31.0
	2400		58.8
	2500		103
Ir-20Re	2200		29.0
	2295		54.8
	2400		103
	2500		183
Ir-30Re	2200		66.0
	2295		122
	2400		236
	2500		412

(b) Corrosion rate on Ir/Re alloys

Figure A.3.1: Ir/Re corrosion properties

Bibliography

[1] Kristina Lemmer, "Propulsion for CubeSats", Acta Astronautica, February 2017

[2] M.M. Finckenor, "Multilayer Insulation Material Guideline", *Marshall Space Flight Center · MSFC, Alabama 35812*, NASA/TP–1999-209263, 1999, pp. 11, 12

[3] Karthik Venkatesh Mani, Francesco Topputo, Angelo Cervone "Chemical Propulsion System Design for a 16U Interplanetary CubeSat", *Politecnico di Milano, Delft University of Technology*, IAC–18–C4.6.2.x47764, 2018

[4] Ampatzoglou A., Kostopoulos V. "Design, Analysis, Optimization, Manufacturing, and Testing of a 2U Cubesat", *Applied Mechanics Laboratory, Mechanical Engineering and Aeronautics Department, University of Patras, Rio Campus, 26500 Patras, Greece*, 2018, p. 4

[5] Timothy A. Collard, J. P. Sheehan, Alec D. Gallimore, "Pressurized Xenon Propellant Management System for the CubeSat Ambipolar Thruster", *University of Michigan, Ann Arbor, MI, 48109, USA*, 2015, pp. 4, 5, 6, 7

[6] Shannah Nichole Withrow, "Program Management for Concurrent University Satellite Programs, Including Propellant Feed System Design Elements", *Ames Research Center, Moffett Field, California*, NASA/TM—2019–220155, 2019, pp. 22, 23, 24, 25, 26

[7] R. Boyer, G. Welsch, and E. W. Collings, "Materials Properties Handbook: Titanium Alloys", *ASM International, Materials Park, OH*, 1994.

[8] Gregg Schneider, "Fundaumentals Of Pressure Regulators", *Emerson Process Management – Regulator Division 310 E. University Dr.McKinney, Texas 75070*, 2007

[9] David Gailey, "Life Expectancy of Compressed Gas Regulators", *The Harris Products Group*

[10] C. Zhang, D. Xing, Y. Li, "Micropumps, microvalves, and micromixers within PCR microfluidic chips: Advances and trends", *MOE Key Laboratory of Laser Life Science Institute of Laser Life Science, South China Normal University*, 26 May 2007

[11] Shabnam Hosseini, "Fatigue of Ti-6Al-4V ", *IntechOpen*

[12] Jasper Bouwmeester, Martin Langer, Eberhard Gill, "Survey on the implementation and reliability of CubeSat electrical bus interfaces", *Faculty of Aerospace Engineering, Delft University of Technology, Institute of Astronautics, Technical University of Munich*, 2016

[13] Stephen A. Jacklin, "Small-Satellite Mission Failure Rates ", *NASA Ames Research Center, Moffett Field, CA*, NASA/TM—2018– 220034, 2018

[14] Gerhard Welsch, Rodney Boyer, E. W. Collings, "Material Properties: Handbook Titanium Alloys", 4^{th} *ed., ASM International*, 2007

[15] B.Dutta, F.H.(Sam) Froe, "The Additive Manufacturing (AM) of Titanium Alloys", *Volume 2, Issue 2*, 2017

[16] L. B. Zang, J. R. White, "Combustion Process of Impinging Hypergolic Propellants", *Marshall Industries, Irvine, Calif. 92664, Lewis Research Center*, Report No. NASA CR-1704, May 1971

[17] Arthur W. O'Brien, Charles L. Caudill, "Design and Fabrication of Hydrazine Storability Test Tank", *Air Force Rocket Propulsion Laboratory, Directorate of Laboratories Air Force Systems Command Edwards Air Force Base, California*, 1969 June

[18] James Paul Mason, Bret Lamprecht, Thomas N. Woods and Chloe Downs, "CubeSat On-Orbit Temperature Comparison to Thermal-Balance-Tuned-Model Predictions", *Volume 32, Number 1*, January 2018

[19] B.R.Lawver, B.P.Breew, "Hypergolic stream impingement phenomena", *NASA-CR-7244*, October 1968

[20] K.Davis, E. Fortner, M. Heard, H. McCallum, H.Putzke, "Experimental and Computational Investigation of a Dual-Bell Nozzle", *Worcester Polytchnic Institute*, April 2014

[21] Miria M. Finckenor, Kim K. de Groh, "Space Enviromental Effects", *NASA ISS Program Science Office*, 2015

[22] Kenneth A. LaBel, "Radiation Effects on Electronics 101:Simple Concepts and New Challenges", *NASA Electronic Parts and Packaging (NEPP) Program*, 2004

[23] G.V.R. Rao, "Exhaust Nozzle Contour for Optimum Thrust", *Jet Propulsion Laboratory*, 1958

[24] Dieter K. Huzel and David H. Huang, "Design of Liquid Propellant Rocket Engines", SP-125, *NASA*, 1967, pp.87

[25] Brian D. Reed, "High-Temperature Oxidation of Iridium-Rhenium Alloys", *NASA, Lewis Research Center, Cleveland, Ohio*, 1995

[26] Hafnium dioxide - Registration Dossier - ECHA [Internet]. Echa.europa.eu. 2020 [cited 30 May 2020]. Available from: https://echa.europa.eu/registration-dossier/-/registered-dossier/12508/4/5

[27] Brian D. Reed, "Evaluation of Oxide-Coated Iridium-Rhenium Chambers", *NASA, Lewis Research Center, Cleveland, Ohio*, 1994

[28] [Internet]. Iridiumrealty.com. 2020 [cited 30 May 2020]. Available from: https://www.iridiumrealty.com/properties/

[29] George P. Sutton and Oscar Biblarz, "Rocket Propulsion Elements", 9^{th} *ed., John Wiley & Sons, Hoboken, New Jersey*, 2017

[30] Califonia Polytechnic State University, "6U CubeSat Design Specification", *The CubeSat Program, Cal Poly SLO*, pp.12

[31] Popp M., Hulka J., Habillah M., Yang V, ”Liquid Rocket Thrust Chambers: Aspects of modeling, analysis, and design”, *Volume 200*, 2004

[32] B.Nuraf, ”A Summary of NASA and USAF Hypergolic Propellant Related Spills and Fires”, *NASA Kennedy Space Center, Engineering Directorate, Fluids Division, Hypergolic and Hydraulic Systems Branch*, 2020

[33] B.Nuraf, ”Hypergolic Propellants: The Handling Hazards And Lessons Learned From Use”, *NASA Kennedy Space Center, Engineering Directorate, Fluids Division, Hypergolic and Hydraulic Systems Branch*, 2020

[34] Yang V., ”Liquid rocket thrust chambers”, Reston, Va.: American Institute of Aeronautics and Astronautics, 2004

[35] S. Gordon and B. J. McBride, "Computer Program for Calculation of Complex Chemical Equilibrium Compositions and Applications", *NASA Reference Publication 1311*, 1996

[36] Waters M. C., ”Analysis Of Additively Manufactered Injectors For Rotating Detonation Engines”, *USAF AFIT-ENY-MS-18-M-301*, 2018

[37] D. Stramaccioni, "The rosetta propulsion system", *Rosetta project team, European Space Agency, ESTEC*

[38] Susana Cortés Borgmeyer, "Chemical Bi-propellant Thruster family", *Ariane Group, Orbital propulsion*

[39] Tang, S.P., and Fenn, J.B., “Experimental Determination of the Discharge Coefficients for Critical Flow through an Axisymmetric Nozzle”, *AIAA Journal, Volume 16, Number 1*, January 1978

[40] Geropp, D., “Laminare Grenzschichten In Ebenen Und Rotationssymmetrischen Laval-duesen”. *Deutsche Luft-Und Raumfart, Forschungsbericht*, 1971, pages 71-90

[41] A.E.Patterson, S.L.Messimer, P.A.Farrington, "Overhanging Features and the SLM/DMLS Residual Stresses Problem: Review and Future Research Need" *University of Alabama in Huntsville*, April 2017

[42] NASA - CubeSats in Orbit After Historic Space Station Deployment [Internet]. Nasa.gov. 2020 [cited 27 May 2020]. Available from: `https://www.nasa.gov/mission_pages/station/research/news/j_ssod.html`

[43] Technology CubeSats [Internet]. Esa.int. 2020 [cited 290 May 2020]. Available from: `http://www.esa.int/Enabling_Support/Space_Engineering_Technology/Technology_CubeSats`